Acta Pharmaceutica Sinica B 2026;16(3):1568−1583

Chinese Pharmaceutical Association
Institute of Materia Medica, Chinese Academy of Medical Sciences

Acta Pharmaceutica Sinica B

www.elsevier.com/locate/apsb
www.sciencedirect.com

ORIGINAL ARTICLE

The transcriptional regulatory network involved in periderm-specific tanshinones biosynthesis in *Salvia miltiorrhiza* root

Yajing Li[a,b,†], Peng Di[c,†], Yinan Zou[a], Xiao Li[a], Ke Zhang[a], Jing Wang[d], Yun Wang[e], Shi Qiu[a], Jingfu Tan[f], Weixu Chen[f], Bo Li[g], Tingzhao Li[g], Lei Zhang[h,*], Ying Xiao[a,*], Wansheng Chen[a,b,*], Junfeng Chen[a,*]

[a]*State Key Laboratory of Discovery and Utilization of Functional Components in Traditional Chinese Medicine, Institute of Chinese Materia Medica, Shanghai University of Traditional Chinese Medicine, Shanghai 201203, China*
[b]*Department of Pharmacy, Changzheng Hospital, Naval Medical University, Shanghai 200003, China*
[c]*State Local Joint Engineering Research Center of Ginseng Breeding and Application, Jilin Agricultural University, Changchun 130118, China*
[d]*College of Life Sciences, Northeast Forestry University, Harbin 150040, China*
[e]*School of Medicine, Shanghai University, Shanghai 200444, China*
[f]*Shangyao Huayu (Linyi) Traditional Chinese Resources Co., Ltd., Linyi 276000, China*
[g]*Amway (China) Botanical R&D Center, Wuxi 214115, China*
[h]*School of Pharmacy, Naval Medical University, Shanghai 200433, China*

Received 20 May 2025; received in revised form 10 October 2025; accepted 29 October 2025

KEY WORDS

Salvia miltiorrhiza;
Tanshinones biosynthesis;
Spatiotemporal metabolic;
Transcriptional regulation network;

Abstract Tanshinones (TAs), well-known specialized diterpenoid metabolites in *Salvia* plants, exhibit distinct tissue-specific production in the root periderm. However, the mechanisms regulating this accumulation pattern remain unknown. Here, we employed a multi-omics analysis strategy to uncover the transcriptional regulatory network responsible for TA biosynthesis in *Salvia miltiorrhiza* roots. By integrating metabolic profiling, RNA-seq, and ATAC-seq, we profile the temporo-spatial dynamics of metabolic, transcriptional, and chromatin landscapes during early root development. Our results demonstrate that TAs biosynthesis and accumulation in *S. miltiorrhiza* roots display spatiotemporal patterns, marked by

*Corresponding authors.
E-mail addresses: 0000002928@shutcm.edu.cn (Junfeng Chen), chenwansheng@shutcm.edu.cn (Wansheng Chen), xiaoyingtcm@shutcm.edu.cn (Ying Xiao), leizhang100@163.com (Lei Zhang).
[†]These authors made equal contributions to this work.
Peer review under the responsibility of Chinese Pharmaceutical Association and Institute of Materia Medica, Chinese Academy of Medical Sciences.

https://doi.org/10.1016/j.apsb.2025.12.018

Chromatin accessibility;
Transcription factor;
Transport;
Gene cluster

periderm-specific accumulation and initiation exclusively at specific developmental stages, tightly coordinated with dynamic changes in chromatin accessibility and transcriptional regulation. The constructed transcriptional regulatory network driving TA biosynthesis was found to be dominated by 211 key transcription factors (TFs). Experimental validations highlighted SmERF105 as a key positive regulator of TA, activating the transcription of *KSL1*, *CYP76AH3*, and the TA transporter *ABCG1* to modulate the TA production. Our study uncovers novel, high-confidence regulators and offers an effective strategy for dissecting the genetic basis of plant specialized metabolites, offering value for advancing TA metabolic engineering.

1. Introduction

Diterpenes, compounds with 20 carbons in their structures, are one of the most common natural product classes. Abietane-type diterpenoids (ATD), a representative diterpenoid class in the *Salvia* genus (Lamiaceae family), have been shown to exhibit various pharmacological activities, such as antitumor, antioxidant, anti-inflammatory, antimicrobial, anti-HIV, cardioactive properties, as well as effects on diabetes and leishmaniasis[1,2]. Tanshinones (TAs) are representative compounds of the phenolic abietanes widely found within the Lamiaceae family and are the bioactive diterpenoid constituents of the traditional Chinese medicinal herb *Salvia miltiorrhiza* (Danshen)[3]. Over eighty tanshinones were identified, which exhibit therapeutically relevant biological activities, including antibiotic, anti-inflammatory, and antioxidant properties, as well as cardioprotective activity[4-7].

ATDs exhibit chemical diversity among lineages. TA and carnosic acid (CA) derivatives constitute two significant classes of ATDs, distinguished by their remarkable lineage-specificities. Concurrently, the two classes of ATDs display distinct distribution patterns, with TAs predominantly accumulating in the periderm of roots and CAs in the aerial parts[8]. Correspondingly, the transcriptional pattern of the biosynthesis pathway has also differentiated, most of which fall into two conserved terpenoid biosynthetic gene clusters (BGC) in Lamiaceae (Supporting Information Fig. S1)[3,9−11]. For instance, copalyl diphosphate synthase 1 (CPS1) and kaurene synthase-like 1 (KSL1) sequentially convert geranylgeranyl diphosphate (GGPP) to miltiradiene, shaping the structural features of ATD within the *Salvia* genus[8,12,13]. However, although KSL1 and CPS1 from different taxa have the same function, their transcriptional patterns are markedly different. In *S. officinal*, for example, they are exclusively expressed in aerial tissues to produce CAs, while in *S. miltiorrhiza*, they are specifically expressed in the root periderm to synthesize TA. Likewise, the CYP76AH, CYP76AK, and CYP71D subfamilies, which have driven ATD diversity across *Salvia* taxa, also exhibit distinctly differentiated transcriptional patterns according to their functional divergence[3,4,8,12-15]. Notably, although the catalytic mechanism for the divergence of the ATD biosynthesis pathway has been almost illustrated, the transcriptional regulation mechanism involved remains unclear. Given the favorable pharmacological activities of TAs and the widespread use of *S. miltiorrhiza* as a raw material for drug development, we investigated the transcriptional regulatory mechanisms of TAs using *S. miltiorrhiza* as a model system. Furthermore, our preliminary study found that the transporter ABCG1 can transport tanshinones and is close to the cluster of tanshinone pathway genes[16]. In plants, the biosynthesis, transport, and storage of secondary metabolites are coordinated processes. It has been observed that in the *Cucurbitaceae* family, a common transcription factor coordinately regulates clusters of transporter and pathway genes[17]. Thus, it is worth investigating whether an efficient regulatory mechanism exists in *S. miltiorrhiza* that coordinates ABCG1 with the tanshinone pathway genes.

Spatiotemporal omics offers high-resolution, precise insights into the regulatory networks of metabolic pathways, especially for compounds exhibiting distinct distribution specificity, developmental stage-specificity, or conditional accumulation. For instance, by integrating metabolomic and transcriptomic profiling from twenty tomato samples of various tissues and developmental stages, a comprehensive metabolic and transcriptomic landscape of tomato growth and development was constructed, accurately identifying SlbHLH114 as a novel positive regulator of the steroidal alkaloid biosynthesis pathway[18]. A dynamic profile of organic acid components during the development of kiwifruit *(Actinidia* spp.) illustrates that AcNAC1 serves as the key regulator of the transporter for citrate to upgrade its accumulation in kiwifruit[19]. Although some multi-omic studies of *S. miltiorrhiza* have predicted multiple TFs to be involved in transcriptional regulation of tanshinones, most have focused on major hormone signaling and environmental factors[20,21]. Therefore, the mechanism governing organ- and tissue-specific biosynthesis of TAs remains largely unexplored, yet they hold great potential for unraveling the underlying regulatory logic of their transcriptional network.

To establish how TAs' metabolism is directed and investigate its underlying transcriptional regulation, we generated a high-resolution temporal and spatial metabolome and transcriptome dataset from different root tissues during early root development stages of *S. miltiorrhiza*. We found a critical "switch" point of TA biosynthesis and demonstrated its accumulation pattern at the root epidermal layers. Correspondingly, the transcriptional profiles and chromatin dynamics revealed the transcriptional network driving TAs biosynthesis during early root development. Additionally, we identified novel TFs, such as ERF105, associated with TA biosynthesis and transport. Our dataset and strategy can be a useful resource for the identification of key regulators of important metabolites in *S. miltiorrhiza* and other medicinal plants.

2. Methods

2.1. Preparation of plant materials

The temporal samples were harvested at 0, 5, 10, 15, 20, 25, 30, 35, and 40 days after seed germination (DAG) of *S. miltiorrhiza* seeds

cultured in a greenhouse. Roots were washed with running water and dried on filter papers, then placed in 1.5-mL centrifuge tubes without RNase. The tubes were immediately frozen in liquid nitrogen and stored at −80 °C, with three replicates for RNA sequencing. Concurrently, *S. miltiorrhiza* roots (4−10 biological replicates) were lyophilized and then subjected to metabolomic analysis for TAs.

2.2. Sample extraction and metabolomic analysis

After freeze-drying, each root samples were crushed into a homogeneous powder, of which 0.01 g was extracted with 1 mL of 80% methanol containing warfarin (200 ng/mL) as an internal reference for 1 h in an ultrasonic bath (53 kHz, 350 W). Each supernatant (final sample) was collected by centrifugation (12,400 × *g*, 10 min).

Analysis of root powders was performed with an Acquity UPLC system (Waters, Milford, MA, USA) equipped with a binary pump, autosampler, and column compartment. The extracted samples were subjected to UPLC with an Acquity BEH C18 column (2.1 mm × 100 mm, 1.7 μm) at 40 °C using gradient elution with solvent A (0.1% formic acid in water) and solvent B (0.1% formic acid in acetonitrile). The gradient was: 5%−20% B over 0−6 min; 20%−22% B over 6−11 min; 22%−60% B over 11−20 min; 60%−65% B over 20−25 min; 65% B over 25−28 min; 65%−95% B over 28−30 min; 95% B over 30−33 min; and finally 95%−5% B over 33−38 min with 5 min additional equilibration at 5% B. The flow rate was 0.40 mL/min, and the injection volume was 1 μL.

The aforementioned UPLC system was coupled to an Xevo G2-XS QTOF (Waters) equipped with an electrospray ionization source. MS was carried out in positive-ion mode using the following instrument settings: sample cone, 30 V; source temperature, 150 °C; desolvation temperature, 450 °C; cone gas flow, 50 L/h; desolvation gas flow, 600 L/h; and capillary voltage, 3 kV. The *m*/*z* range was 50 to 1200 with a scan time of 0.35 s. The low collision energy was set to 6 eV, and the high collision energy was steadily increased from 15 to 30 eV. A sodium formate solution (0.5 mmol/L) was used to calibrate the instrument. Raw MS data collected in continuum mode were analyzed using UNIFI software (Waters), and raw mass spectra acquired in centroid mode were analyzed by MS-DIAL v 4.20 (http://prime.psc.rik en.jp/compms/msdial/main.html). The mass spectra were viewed with MassLynx v 4.2 (Waters). TAs were identified based on the compound library of *S. miltiorrhiza* we had constructed previously[22].

2.3. RNA-seq and data processing

A total of 42 transcriptome profiles from five tissues in mature roots and nine developmental stages of seedling roots were obtained by RNA-seq using the Illumina NovaSeq6000 sequencing (150 bp, paired-end, Shanghai Biozeron Co., Ltd., Shanghai, China). The expression level for each gene was calculated using the fragments per kilobase of exon per million mapped reads (FRKM). K-means cluster analysis of genes was performed in R (v4.4.3) using Z-scaled FPKM, and the gene expression heat map was displayed using the R package ComplexHeatmap (v2.4.3). The identification and family classification of TFs were predicted on the PlantTFdb website (http://planttfdb.gao-lab.org/). Differentially expressed genes were identified using limma, with a P value < 0.01 and FDR < 0.01 as the criteria for significance. The enrichment analysis of TF families was achieved using the enricher function in the R package clusterProlifer (v3.16.1)62.

Pseudotime analysis was conducted with minor modifications to previously published methods[23]. PCA was first applied to all expressed genes to distinguish samples. Next, the Euclidean distances between neighboring samples along the developmental trajectory were measured to generate developmental time units, standardized on a scale from 0 to 10. For each gene, the *Z*-scaled expression values were interpolated into 500 points along its pseudotime trajectory using the loess function in R (v4.4.3), enabling smooth and continuous comparisons. Gene clustering and heatmap visualization were performed with mfuzz and ComplexHeatmap, respectively.

2.4. Correlation network of transcription factors and pathway genes

The mean transcription levels for stage 1 (0−20 DAG) and stage 2 (25−40 DAG) were calculated as temporal data. Expression matrices from various tissues were then merged. Using R (v4.4.3), the Pearson correlation coefficients were determined. Correlations with values exceeding 0.9, below −0.9, and a P value < 0.01 were retained. Finally, the network was visualized with Cytoscape[24].

2.5. ATAC-seq and data processing

For ATAC-seq data, the quality of the raw data was first assessed using fastqc software. The raw data were then aligned to the reference genome using the bowtie2 software[25]. Then, MACS2 was used to perform peak calling on each sample[26]. After that, we performed genomic position annotation, motif analysis, and GO and KEGG enrichment analyses of the target genes in the peaks' region. The peaks were visualized using IGV software[27].

2.6. Isolation and analysis of SmERF105

Total RNA was extracted from 6-month *S. miltiorrhiza* roots and used to construct a complementary DNA (cDNA) library as the template. The primers were designed from the *S. miltiorrhiza* genome database (Supporting Information Table S1). The PCR products were electrophoresed in a 1% agarose gel, and the target fragments were eluted, then cloned into Blunt-zero vectors and transferred into the Trans1-T1 cell, further sequenced by Suzhou Genwiz, China.

2.7. Protein subcellular localization

The open reading frames (ORF) of SmERF105 were cloned into the pEAQ-GFP-HT vectors using Xho I and Age I sites. The prepared plasmids were introduced into the *A. tumefaciens* strain GV3101. The results were recorded after 2 days of transformation with the emission wavelength in the range of 488−510 nm. The GFP fluorescence signal was imaged using a Leica TCS SP5 laser confocal scanning microscope (Leica Microsystems, Wetzlar, Germany).

2.8. Yeast one-hybrid assay

The promoter fragments containing GCC cis elements were amplified by PCR using specific primers (Table S1). The amplified promoter fragments and the muted sequences were cloned into the pLacZ vector as baits, and the full-length CDS of *ERF105* was fused at the C terminus of GAL4-AD in the pB42AD vector to construct the prey. The prepared prey and bait vectors were

transformed into the yeast strain EGY48. Additionally, combinations of the empty vector pB42AD and the prepared pLacZ vectors, the pB42AD with *ERF105* and the pLacZ vector with muted sequence were transformed into the yeast strain EGY48 as the negative control, respectively. The SD/Trp/Ura plates with appropriate nutrients were used to screen the transformants, and the positive clones were grown on SD/Trp/Ura plates with X-gal for determining the protein-DNA interaction based on the blue color development.

2.9. Electrophoretic mobility shift assays

The *SmERF105* was cloned into the pEGX-4T-1 vector to produce GST-tagged fusion proteins. The pEGX-4T-1-*SmERF105* constructs, and negative control empty vectors, were transformed into the *E.colistrain* transcetta DE3 (TransGen Biotech). Then, 0.5 mmol/L isopropyl β-D-1-thiogalactopyranoside was used to induce the expression of the fusion protein for 16 h at 16 °C. AKTA pure chromatography systems (GE Healthcare) were used to purify proteins.

The DNA probes used in this experiment were synthesized by Genewiz (Suzhou, China). The primers and probes are listed in Table S1. Electrophoretic mobility shift assays (EMSAs) were performed using the EMSA/The Gel-Shift Kit (Thermo Scientific™, USA) following the manufacturer's instructions. After blotting on a positively charged nylon membrane, an ultraviolet (UV) cross-linker was used to cross-link the DNA. The biotin-labeled DNA was detected by chemiluminescence.

2.10. Transient dual-luciferase reporter assay

Transient expression assays were performed in *N. benthamiana* leaves. The *KSL1*, *ABCG1*, and *CYP76AH3* promoters were cloned into the pGreenII 0800-LUC to generate the reporter constructs *ABCG1pro: LUC*, *KSL1pro: LUC*, and *CYP76AH3pro: LUC*, and *SmERF105* was cloned into the pGreenII 62-SK to generate the effector construct *35Spro: SmERF105*. A low-light cooled CCD imaging apparatus (NightSHADE LB985; Berthold; Germany) was used to capture the LUC image and quantify luminescence intensity. The leaves were sprayed with 150 μg/mL Beetle luciferin and were placed in the dark for 7 min before luminescence detection with three independent experiments. Relative LUC activity was statistically analyzed using WINVIEW32 software. In addition, the quantitative results were performed using the Dual-Luciferase® Reporter Assay System (with Renilla internal reference normalization).

2.11. Vector construction and generation of transgenic lines

We screened dual knockout sites of *SmERF105*, each 20 bp in length (gRNA1: CCTTCAACCCCTTATATAAA, gRNA2: CAGCTCTTGATCTCATACGC), and co-constructed them into the CRISPR/Cas9 system. This system was developed by replacing the Cas9 promoter in the previously described Yang et al. system with the tomato *EF1a* promoter[28,29] (Supporting Information Fig. S2). Transform the positive vectors to GV3101 and induce the formation of callus tissue through leaf disc transformation, which then differentiates into shoots. Cut and insert the shoots into 1/2 MS medium for rooting. Extract DNA from the regenerated plants, amplify the fragment containing the knockout sites with primers (Table S1), and perform sequencing to verify the gene knockout. Obtain three gene knockout lines. After being cultured in a greenhouse for 45 days, the roots were collected for metabolite detection and qRT-PCR assays.

2.12. Expression analysis of the pathway genes by quantitative real-time PCR

Transgenic *S. miltiorrhiza* plants were obtained *via Agrobacterium* infestation of a leaf disc. Total RNA was extracted (Trans Gen Biotech, Beijing, China) and reversed transcription to get cDNA library (Takara, Cat. No. 6210B). PCR were performed using QuantStudio 3 by TB Green Premix Ex Taq II (Takara, Cat. No. RR820A). Three independent lines were used in these experiments for gene expression analyses. The primers used here are shown in Table S1.

2.13. Quantification of tanshinones by UPLC−MS/MS

Cryptotanshinone, Tanshinone IIA, Tanshinone I, and dihydrotanshinone I were quantified with a UPLC system (Agilent 1290 Infinity, California, USA) coupled with a G6460A triple-quadrupole mass spectrometer. An Acquity UPLC Xselect CST C18 column (50 mm × 2.1 mm, 2.5 μm) was used for separation. The binary gradient of water containing 0.1% formic acid/2 mmol/L ammonium acetate (buffer A) and acetonitrile (buffer B) at a constant flow rate of 0.3 mL/min was applied with an injection volume of 5.0 μL. The column oven temperature was 35 °C. A linear gradient was used: 60% B over 0−6.5 min, and 60%−90% B over 6.5−10.0 min. The mobile phase was returned to 60% B over 3 min, with 3 min re-equilibration. MS spectra were acquired in positive-ion mode, which was carried out through multiple reaction monitoring scans with optimization of the product ion obtained from the fragment of the isolated precursor ion for each analyte (Supporting Information Table S2). MS parameters were set according to a previous study[16].

3. Results

3.1. The spatiotemporal accumulation patterns of tanshinones in S. miltiorrhiza roots

We first observed the TA accumulation pattern in *S. miltiorrhiza* roots during early developmental progress, spanning from 0 to 40 days after germination (DAG) (Fig. 1A). In the initial stages after germination (about 0−10 DAG), TA accumulation was absent in the root, which appeared white. Around 25 DAG, TA accumulation was observed in epidermal cells, which represented red patches owing to the conjugated structure of tanshinones. With increasing TA accumulation, the root displayed a dark red color at 40 DAG. The time course phenotype variation of the root indicated the biosynthesis pattern of TAs. We further featured metabolic profiles of multiple TA metabolites. Root samples were collected every five days after germination and were analyzed using liquid chromatography-tandem mass spectrometry (LC−Q/TOF−MS). Twelve TA metabolites were identified in total (Supporting Information Table S3), which were relatively quantified with 0 DAG samples as a control. As results showed, all TA metabolites could hardly be observed during 0−20 DAG and accumulated after 25 DAG (Fig. 1B). Take tanshinone IIA, the most utilized tanshinone component in pharmaceuticals, its

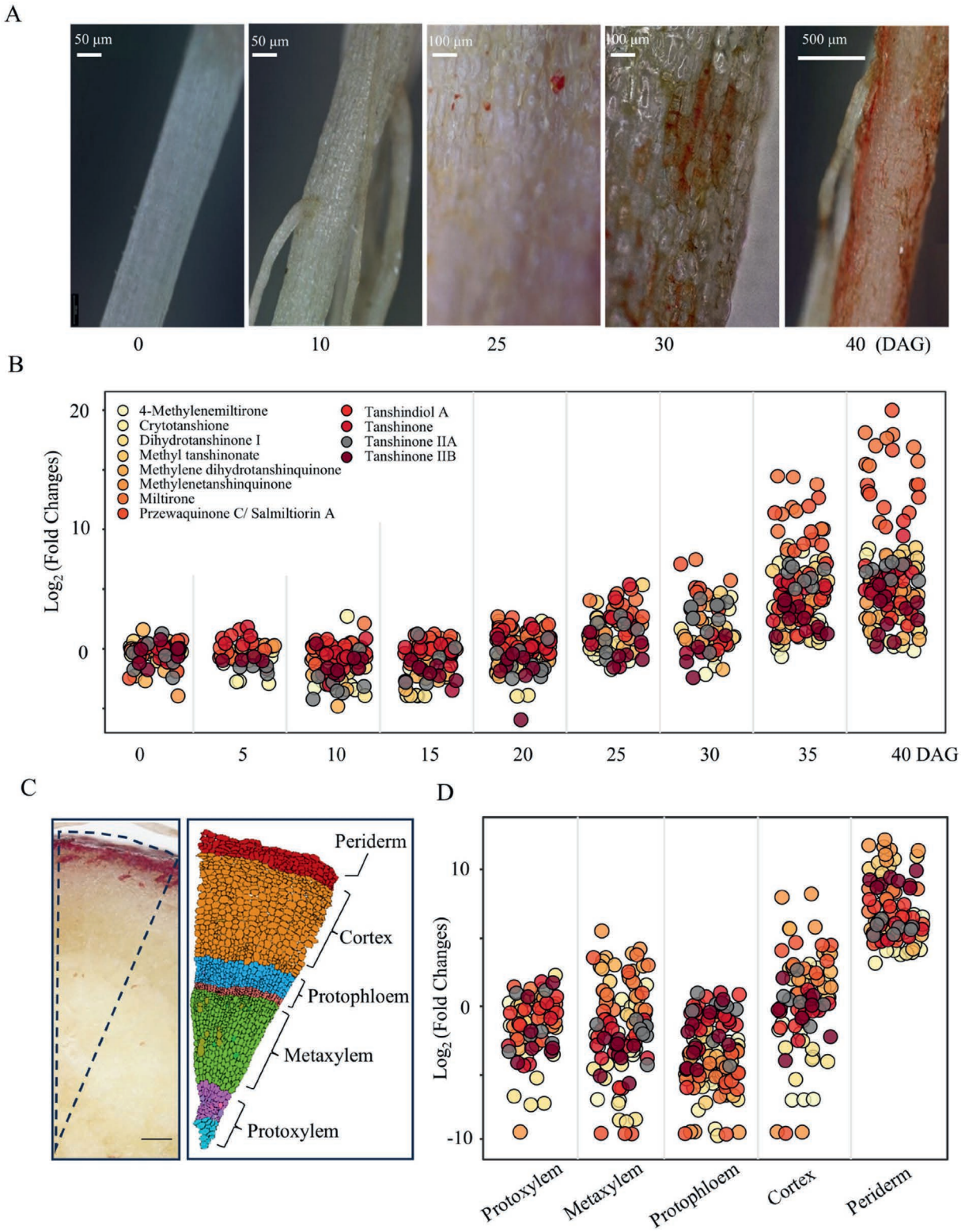

Figure 1 The temporal and spatial accumulation patterns of tanshinone-related metabolites in *S. miltiorrhiza* roots. (A) The appearance of the roots during the early developmental period was observed by a 3D digital microscope. (B) The temporal metabolic profiling of tanshinones in *S. miltiorrhiza* roots during early development stages (0−40 days after germination, DAG). The fold changes of relative abundance level (in $\log_2$ fold change) of twelve tanshinone metabolites were represented by different colors. The profiles of each metabolite can be found in Supporting Information Table S1. (C) The accumulations of tanshinones were only observed in the periderm *S. miltiorrhiza* root. The tissue types of *S. miltiorrhiza* root were profiled in the right panel, which was generated using ggPlantmap[55]. Scale bar = 50 μm. (D) The spatial metabolic profiling of tanshinones in different *S. miltiorrhiza* root tissues. The relative abundance level (in $\log_2$ value) of twelve tanshinone metabolites. The profiles of each metabolite can be found in Supporting Information Table S2.

relative abundance increased by over 300-fold during the time course.

Besides, the color phenotype was only displayed on periderm layers (Fig. 1C), indicating a unique spatial accumulation pattern of TAs. The TA metabolites were further profiled. According to the secondary root structure, the six-month-old mature *S. miltiorrhiza* roots were manually separated into five distinct spatial sections for metabolic profiling, from outer to inner layer: periderm, cortex, protophloem, metaxylem, and protoxylem (Fig. 1C). Consistent with the observed phenotype, all detected TAs exhibited dominant accumulation in the periderm layers (Fig. 1D and Supporting Information Table S4). Thus, we supposed a regulatory "switch", which turns on the TA biosynthesis pathway at a certain developmental stage specific to root periderm.

3.2. The temporal transcriptome atlas during the development stages of S. miltiorrhiza roots

Corresponding to the temporal metabolic profiling, the transcriptome landscape of *S. miltiorrhiza* roots was generated. A total of 27 transcriptome libraries were generated for nine time course samples with three replicates per period (Supporting Information Table S5). Transcript features were analyzed first. As a result, the percentage of transcribed loci ranged from 48.91% to 58.53% among all 29,236 loci annotated from the *S. miltiorrhiza* genome, and their overall transcriptional level was also in a similar range (Fig. 2A and B). To further feature the transcriptional dynamics of root development, pseudotime analysis was performed, based on principal-component analysis (PCA) distance[23], to display the temporal order of gene expression (Fig. 2C). A clear sequential

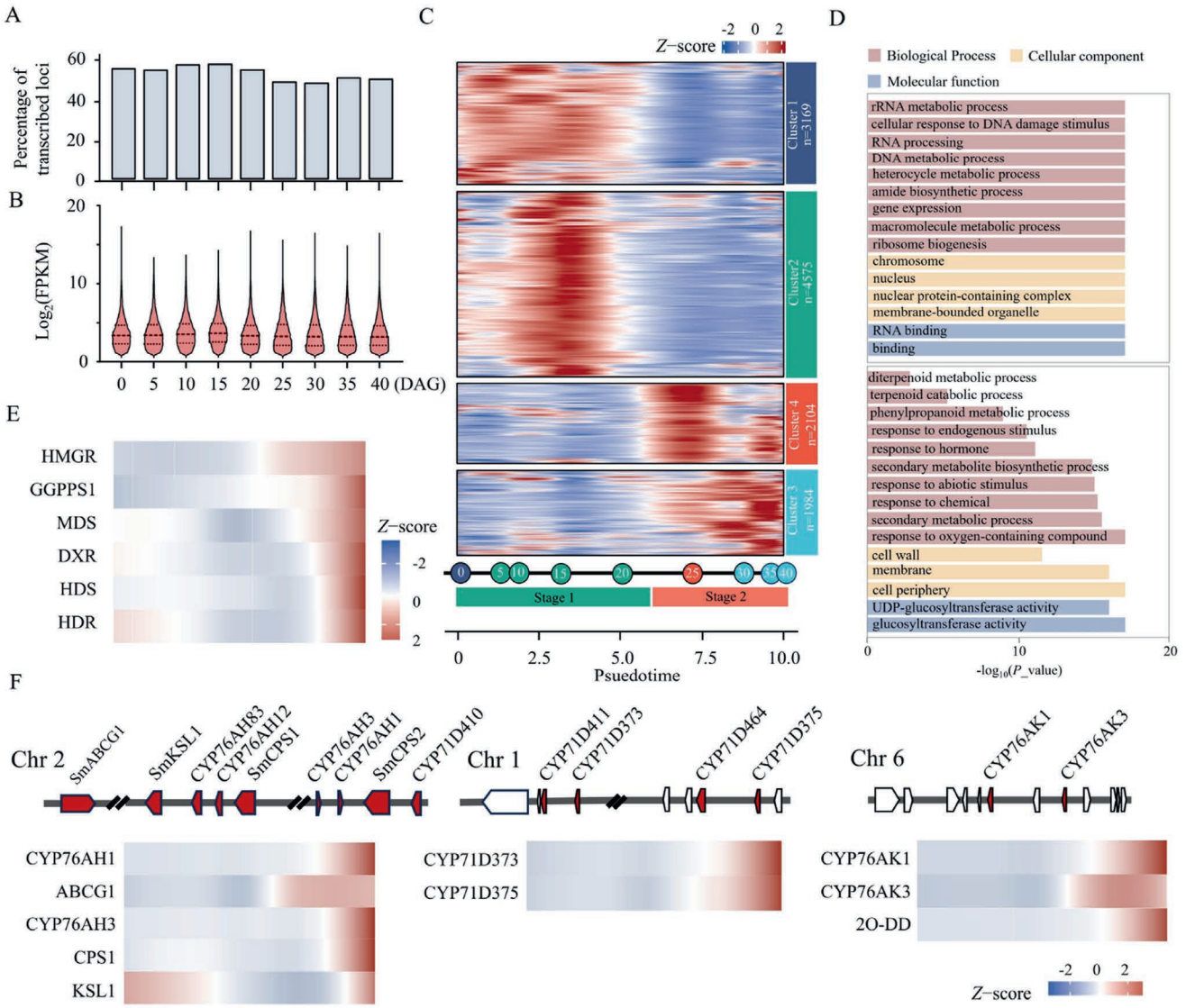

Figure 2 The temporal transcriptome profiling during development stages of *S. miltiorrhiza* roots. (A) Transcriptome-wide distribution of transcribed loci in each temporal sample. (B) The temporal transcript levels of *S. miltiorrhiza* roots during early development stages (0−40 days after germination, DAG). (C) Temporal transcriptome of the roots using pseudotime analysis. (D) GO enrichment of genes that are highly expressed in two distinct developmental stages. (E) Expression of six genes involved in the diterpenoid pathway shows a co-expression pattern with TA accumulation. (F) Transcriptional features of TA biosynthetic genes that are located in three BGCs.

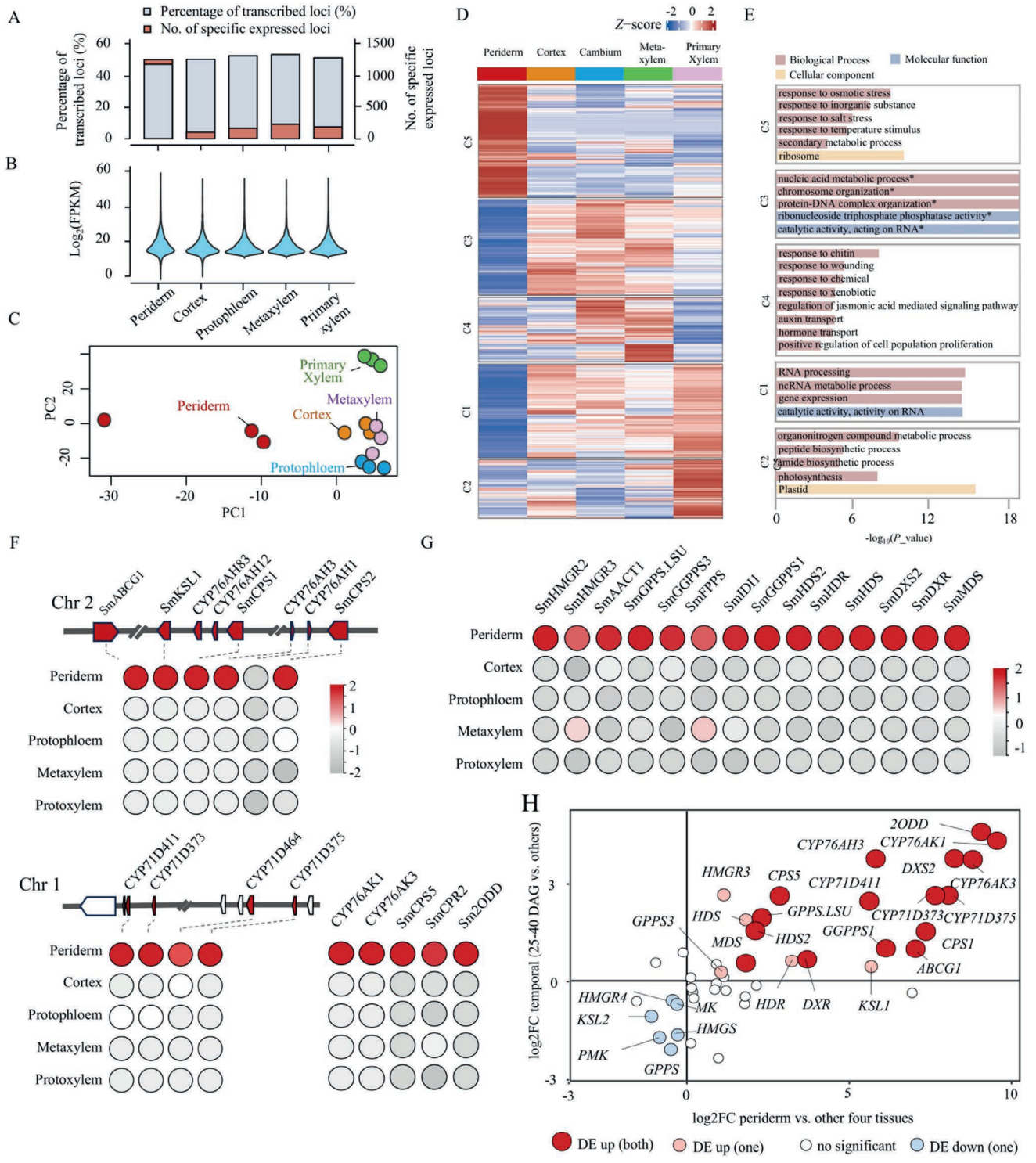

Figure 3 The spatial transcriptome profiling of *S. miltiorrhiza* root tissues. (A) Transcriptome-wide distribution of transcribed loci in each tissue sample. (B) The distribution of transcript levels in each root tissue. (C) PCA analysis of spatial RNA-seq data, three replicates were sequenced for each dissected root tissues. (D) Heatmap of tissue-specific highly expressed genes sorted by k-means clustering. All different expressed genes (DEG) were grouped into five clusters (C1−C5). (E) GO enrichment of genes in clusters 1−5. (F) The transcriptional features of BGCs involved in TA biosynthesis in different tissues. (G) Fourteen diterpenoid pathway genes are highly transcribed in the periderm of the root. (H) Fold change-fold change (FC−FC) plot showing the $\log_2$ fold changes of differentially expressed genes (DEGs) in spatial variations (periderm *vs.* other four tissues, *x*-axis) and temporal variations (25−40 DAG *vs.* others, *y*-axis).

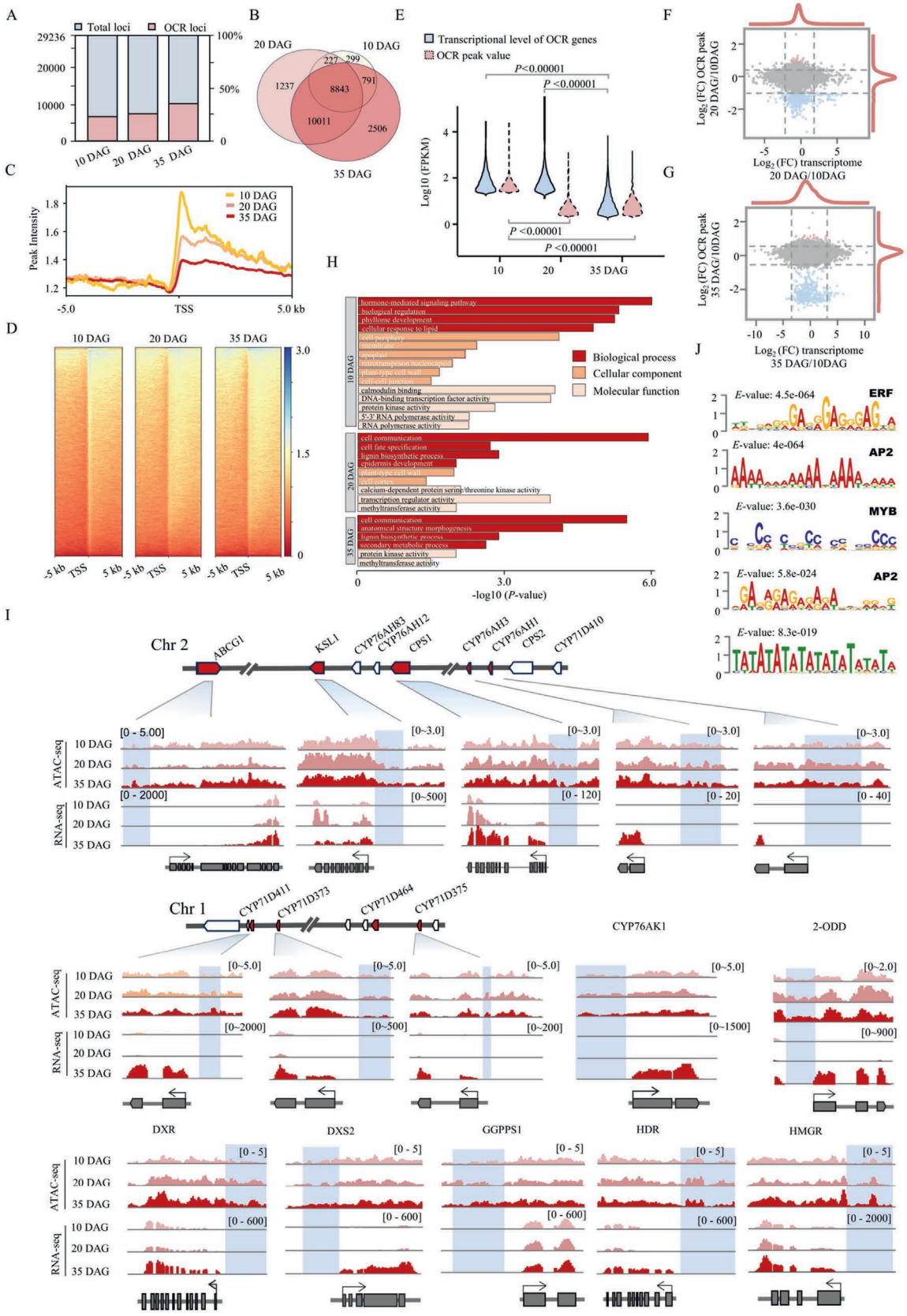

Figure 4 The temporal variation for chromatin accessibility during the development of *S. miltiorrhiza* roots. (A) Distribution of open chromatin regions (OCR) across all loci on the *S. miltiorrhiza* genome at 10, 20, and 35 DAG. (B) The similarities and differences of chromatin open sites in three periods. (C, D). Peaks distribution for OCRs along the genic region, TSS: transcription start site. (E) Changes in overall chromatin openness levels and transcription levels. (F, G) A scatter plot of 9-quadrant associate analyses shows the correlation between transcription and OCR. (H) GO

time-serial expression pattern identified the time course into two distinct stages. Clusters 1 and 2 (0−20 DAG) encompassed two distinct early high-expression transcription patterns (7744 genes), while the remaining samples (25−40 DAG) represented two distinct clusters with 4008 highly expressed genes in total. Although the overall counts of expressed genes showed minimal variation across the observed developmental stages (Fig. 2A), the perturbations of highly expressed genes were markedly significant. We utilized Gene Ontology (GO) enrichment to explore the majority of physiological processes (Fig. 2D). The most significant GO terms were involved in the processes of transcription and translation, such as RNA processing (GO:0006396), nuclear protein-containing complex (GO:0140513), rRNA metabolic process (GO:0016072), and ribosome biogenesis (GO:0042254), indicating that tissue proliferation might dominate the early stages of root development. Subsequently, secondary metabolic processes such as diterpenoid metabolic process (GO:0016101), phenylpropanoid metabolic process (GO:0009698), and glucosyltransferase activity (GO:0008194) became enriched after 25 DAG, corresponding to the accumulation pattern of TAs. As expected, the TA biosynthesis pathway showed a similar transcriptional profile. Gene families involved in the common upstream diterpenoid pathway genes (*HMGR*, *GPPS1*, *MDS*, *DXR*, *HDS*, *HDR*) exhibit transcriptional patterns identical to TA accumulation (Fig. 2E). Notably, all functionally validated genes involved in TA biosynthesis primarily fall into three biosynthetic gene clusters (BGC)[3,13-15], which were highly expressed at the late stages (Fig. 2F).

3.3. The spatial transcriptome atlas of S. miltiorrhiza root

We also generated a spatial transcriptome map for *S. miltiorrhiza* root tissues to elucidate the transcriptional mechanism of unique TA accumulation in the periderm. The mature roots (6-month-old) were manually separated for sequencing (Table S5). The overall transcriptional profile was analyzed first. The number of transcribed loci was similar in all tissues, ranging from 50.09% to 53.92% (Fig. 3A). However, the genes with tissue-specificities varied significantly, with 1256 genes in periderm, whereas other tissues exhibited far fewer, only ranging from 73 to 235 (Fig. 3A). We also found that the overall transcription level range in the periderm and cortex is higher than in other tissues (Fig. 3B). PCA showed that the plots represented periderm and primary xylem samples were separated from the others, indicating their distinctly unique transcriptional profile (Fig. 3C).

The general transcriptional variation between each tissue was displayed according to a trend analysis, grouping all examined transcripts into five distinct clusters (C1−C5) to characterize each tissue (Fig. 3D). As shown, the transcription in periderm was unique, with the most highly expressed genes enriched in C5. Cortex, cambium, and metaxylem were similar in transcription, and most of the specific genes for primary xylem fell into C1 and C2. GO annotation was performed to further elucidate the transcriptional traits and physiological properties of each cluster (Fig. 3E). For example, the enriched categories in periderm (C5) were mostly related to abiotic stress responses, such as osmotic stress (GO:0006970), inorganic substance (GO:0010035), and salt stress (GO:0009651), representing the armor-like role of root periderm. The terms related to secondary processes were also enriched in this cluster. In addition, the transcriptional pattern of catalytic genes involved in TA biosynthesis was profiled. Almost all validated genes involved in TA metabolism showed a unique spatial expression pattern in the periderm with high transcription level (Fig. 3F and G). For upstream terpenoid gene families, particularly those involved in pathways such as the mevalonic acid (MVA) and methylerythritol phosphate (MEP) pathways, with a putative role in diterpenoid biosynthesis, some members exhibited significant periderm-specific expression, providing additional evidence for their specific involvement in TA biosynthesis (Fig. 3G).

The temporal and spatial transcription profiles of the TA biosynthesis pathway were compared, as illustrated by the fold change (FC) plot. Sixteen pathway genes are significantly highly expressed in both spatial and temporal dimensions, and five genes are highly differentially expressed in one dimension (Fig. 3H and Supporting Information Table S6). Ten upstream genes, comprising six MEP pathway genes (*HDS*, *HDR*, *DXS2*, *DXR*, *HDS2*, *MDS*), one MVA pathway gene (*HMGR3*), *GPPS3*, *GPPS.LSU*, and *GGPPS1* exhibited a transcriptional profile consistent with TA accumulation. Specifically, their expression was temporally highest at 40 DAG and spatially predominant in the periderm (Fig. 3H and Table S6). Ten downstream genes (*KSL1*, *CPS1*, *CPS5*, *CYP76AH3*, *CYP71D411*, *CYP76AK1*, *CYP76AK3*, *CYP71D375*, *CYP71D373*, and *2ODD*) and the transporter gene ABCG1 were differentially expressed under at least one dimension. Their observed expression patterns corroborated their established roles in TA biosynthesis and transport (Fig. 3H and Table S6). This co-expression pattern implies that these genes play critical roles in TA biosynthesis within the complex terpenoid metabolic network.

3.4. The dynamic landscape of open chromatin during S. miltiorrhiza root development

Chromatin accessibility is a prerequisite for gene expression and regulation. To uncover the open chromatin regions (OCRs) associated with TA metabolism during root development, transposase-accessible chromatin with sequencing (ATAC-seq) was performed to assay OCR profiles. Three temporal points (10, 20, and 35 DAG) with the most significant variation were selected for sequencing, generating 86,361,882, 97,141,746, and 115,662,420 mapped reads for each time point (Supporting Information Table S7). After mapping to the genome, the average OCR peak at each time point was 69,862, 89,996, and 110,004, corresponding to 8701, 10,649, and 16,172 loci, respectively, within the 29,236 loci of the *S. miltiorrhiza* genome. This reflects an increasing proportion (29.23%−55.32%) of OCR genes during the root development (Fig. 4A). Additionally, 299, 1237, and 2506 unique OCR genes were identified in the samples from each time series (Fig. 4B). The distribution of peaks was found to be enriched near the transcription start site (TSSs), with decreasing peak intensity along with the time series (Fig. 4C and D). We also found that the transcripts of OCR genes were primarily associated with OCR level, while the 20 DAG sample showed less consistency (Fig. 4C and E). A scatter plot of the nine-quadrant association analysis was performed and showed the strong correlation between transcription and OCR level (Fig. 4F and G). Notably, the

functional enrichment of genes associated with open peaks in three periods. (I) The openness Dynamic OCR (top) and transcriptome (bottom) modification tracks for TA biosynthetic genes. (J) ERF, AP2, and MYB are the most prominently related to the TF family.

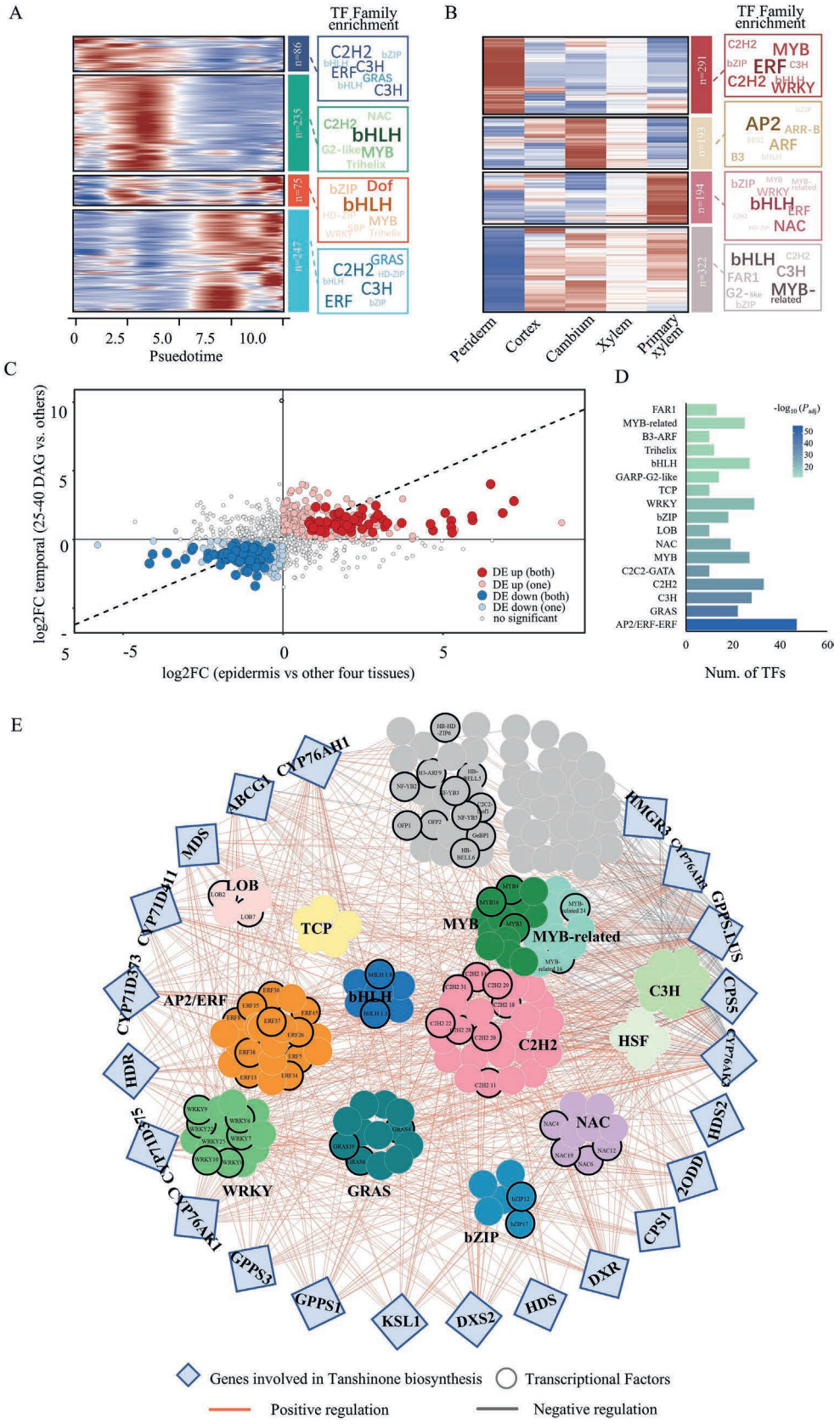

Figure 5 The transcriptional regulatory network for tanshinone biosynthesis. (A) Temporal transcription pattern of transcription factors (TFs) inferred from pseudotime analysis (Fig. 2C). These TFs were clustered into four distinct categories. The right panel displays word clouds representing the most significantly enriched TF families. (B) Spatial transcriptional pattern of TFs in different root tissues. (C) FC−FC plot illustrating the spatial (periderm *vs.* others) and temporal (25−40 DAG *vs.* others) $\log_2$ fold changes of differentially expressed TFs. (D)

decrease in OCR level didn't lead to a comprehensive reduction in transcriptional level, particularly in 35 DAG samples. This suggests the involvement of additional regulatory mechanisms, such as histone and DNA modifications, and highlights the regulatory diversity[30,31].

According to developmental stages, the main functions of OCR genes were different (Fig. 4H). In 10 DAG, GO enrichment for OCR genes is mainly related to growth and primary metabolism, *e.g.*, hormone-mediated signaling pathway and DNA-binding transcription factor activity. OCR genes in 20 DAG were mainly associated with root tissue differentiation, such as cell fate specification and epidermal development. The secondary metabolic-related processes didn't become active until 35 DAG. The OCRs for TA-related genes, including catalytic and transporter genes, were analyzed (Fig. 4I). The transcription variation in several genes, including *ABCG1*, *KSL1*, *CPS1*, *CYP71D*, *2-ODD*, and *DXR*, was found to be strongly correlated with the dynamic OCR patterns in their promoter regions, suggesting that chromatin feature changes significantly impact the expression dynamics of TA biosynthesis. Additionally, we analyzed the putative binding motifs enriched in promoter regions of these TA genes, identifying ERF, AP2, and MYB as the most prominently involved TF families (Fig. 4J).

3.5. The temporo-spatial transcription regulation network revealed the key regulators of TA biosynthesis

The genome-wide identification of TFs in *S. miltiorrhiza* discovered 1815 TFs from 66 families in total, according to the PlantTFDB[32] (Supporting Information Table S8). Temporal transcription profiles of 1163 root-expressed TFs were clustered into four groups, consistent with the overall transcription landscape (Fig. 5A). Family enrichment analysis revealed the most active TF families in each developmental stage. We focused on the cluster for the late stage of the pseudotime trajectory, involving 247 TFs, and found ERF, C3H, C2H2, and GRAS TFs were most enriched. Based on the spatial transcription profiles of TFs, four major modules were categorized, with 291 TFs highly expressed in the periderm, including the predominantly enriched families as MYB, ERF, WRKY, and C2H2 (Fig. 5B). Subsequently, the tempo-spatial TF profiles were integrated and visualized using FC-FC plots. The analysis highlighted distinct expression patterns: 57 TFs exhibited high expression in the periderm and at the late developmental stage of the root; 91 TFs showed significantly low transcript levels under the same conditions; 154 TFs were highly expressed in only one dimension (either space or time); and 205 TFs displayed low expression in a single dimension (Fig. 5C, Supporting Information Table S9). We further ranked these 507 TFs exhibiting significant transcriptional variation according to their engagement (Fig. 5D). The AP2/ERF family emerged as the most enriched TF family, with ERF6, ERF8, and ERF106 having been previously reported as regulators of TA biosynthesis[33-35].

We further constructed a transcriptional correlation network including 507 TFs and different transcript pathway genes (coefficient threshold >0.9 or < -0.9, and $P < 0.01$) (Fig. 5E). 211 TFs were involved with at least one synthetic gene, including 123 TFs with positive correlation, and 88 TFs with negative correlation with the TA biosynthesis pathway. According to current literature, TFs known to regulate tanshinone biosynthesis primarily belong to families such as ERF, WRKY, bHLH, bZIP, MYB, NAC, and GRAS[20,21]. Therefore, we focused on TFs from these families within the co-expression network. Widespread significant positive correlations were observed between TFs and multiple tanshinone biosynthetic genes, particularly within the ERF, WRKY, NAC, and MYB families, consistent with previous reports. It indicates their potential roles in regulating tanshinone biosynthesis and transport. However, it should be noted that positive correlation does not necessarily imply direct regulation. These TFs may function indirectly through interactions with other TFs or hormonal signals. Within the network, the ERF family was the most represented with 22 members, followed by WRKY (16), MYB (13), GRAS (12), NAC (9), bHLH (7), and bZIP (6) (Supporting Information Fig. S3). Furthermore, enrichment analysis revealed that the ERF family was the most significantly enriched (Fig. 5D). Thus, we prioritized the ERF family for further investigation. Among the 22 ERF members, ten were differentially expressed in both temporal and spatial dimensions and marked with a black border in the network, which might correspond to their involvement in programmed transcriptional regulation during root development or a switch-like role in tissue-specific regulation.

Genes specifically involved in TA metabolism, including four biosynthetic genes (KSL1, CPS1, CYP76AH1, and CYP76AH3) and one TA transporter gene (ABCG1), were selected as target genes. The promoters of the five genes contain GCC-box cis elements to which the ERF family TFs bind (Supporting Information Fig. S4). We successfully cloned seven of the ten TFs to screen their regulatory role towards TA biosynthetic genes *via* yeast one-hybrid (Y1H) (Supporting Information Table S10). As a result, binding affinities of SmRAP2-1 and SmERF039 towards KSL1 *in vitro* were observed, while ERF105 can bind to GCC-box motifs on the promoter of CYP76AH3, KSL1, and ABCG1 (Fig. 6A, Supporting Information Figs. S5 and S6). In addition, the ATAC-seq profiles showed that the chromatin accessibility of SmERF105 is enhanced at the late developmental stage, which is consistent with its high transcript level, as well as the three target genes (Fig. 4I, Supporting Information Fig. S7).

3.6. ERF105 is a novel positive regulator for tanshinones biosynthesis and transport

Using the strategy described above, we expanded our discovery for transcription factors that regulate TA metabolism. We found that ERF105 might exert dual roles on both biosynthesis and transport of TAs according to the Y1H result (Fig. 6A); it was selected for further functional validation. The electrophoretic mobility shift assays (EMSA) were performed using purified heterologously-expressed ERF105, and the fragments containing GCC motifs in the promoters of *KSL1*, *CYP76AH3*, and *ABCG1*

Enrichment analysis showing the AP2/ERF−ERF family as the most dominant and significant among the differentially expressed TFs. (E) Transcriptional regulation network according to Pearson correlation between TFs and TA biosynthesis pathway genes. TF families are distinguished by color. The significant correlation (correlation coefficient >0.9 or < -0.9, and P value < 0.01 as criteria) between each gene pair is represented by red line for positive correlation, and gray lines for negative correlations. The black border indicates the TFs that are highly expressed both during the late developmental stage of the root and in the periderm, with gene names labeled.

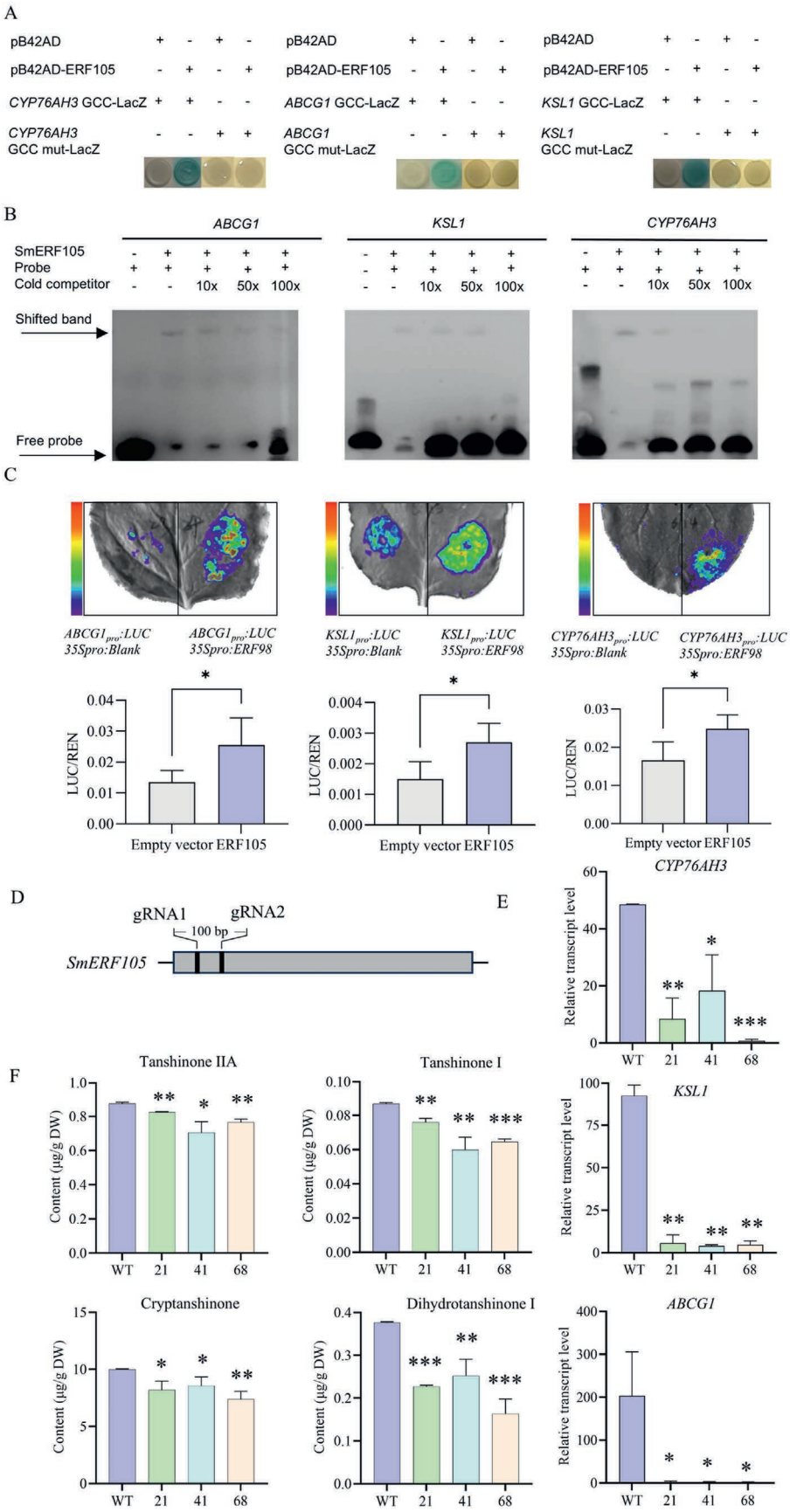

Figure 6 ERF105 is a key regulator involved in the spatiotemporal biosynthesis of TA. (A, B). Yeast one-hybrid analysis (Y1H) and electrophoretic mobility shift assay (EMSA) showing ERF105 can bind the GCC box in the promoters of *CYP76AH3*, *ABCG1,* and *KSL1*.

were labeled with biotin as probes. The result confirmed the direct binding of ERF105 to probes derived from *KSL1*, *CYP76AH3*, and *ABCG1 in vitro* (Fig. 6B). We further verified the *in vivo* binding and regulation of ERF105 using a Dual-luciferase (LUC) reporter assay in *tobacco* leaves (Fig. 6C). The results showed that SmERF105 could activate the promoters of *KSL1*, *CYP76AH3*, and *ABCG1*. The quantitative assays further showed that ERF105 can significantly activate the expression of *ABCG1*, *KSL1*, and *CYP76AH3*, which is consistent with the fluorescence results observed in tobacco leaves (Fig. 6C). Taken together, this evidence of protein-DNA interactions strongly suggests ERF105 as a positive regulator of TA metabolism.

To investigate the role of SmERF105 in TA biosynthesis, *in vivo* functional validations were conducted. We first demonstrate the sub-cellular location of SmERF105 through transient expression in *tobacco* leaves, revealing its nuclear and cytoplasmic localization as a typical TF (Supporting Information Fig. S8). To further illustrate the regulatory role of SmERF105, CRISPR-Cas9-mediated knockout mutant *erf105* lines were generated. Two target regions near the 5′-end, spaced 100 bp apart, were selected for a dual knockout of the target loci (Fig. 6D). Three mutant lines were obtained (Supporting Information Fig. S9). Line 21 is a homozygous mutant, while lines 41 and 68 carry biallelic mutations at different sites (Fig. S9). The transcription of proposed target genes, *KSL1*, *CYP76AH3*, and *ABCG1*, was detected first by qRT-PCR. As expected, the transcription level of genes significantly decreased in all *erf105* lines, with *SmABCG1* exhibiting the most pronounced downregulation by 97.2-fold, supporting the role of ERF105 as a positive regulator. Correspondingly, TA contents were significantly reduced in each *erf105* strain as well, with four examined TA metabolites marked decreased: tanshinone by 5.6%−19.4%, tanshinone I by 12.5%−30.1%, cryptotanshinone by 18.2%−26.0%, and dihydrotanshinone I by 32.9%−56.6% (Fig. 6E and F). The above results indicate that SmERF105 may serve as a novel positive regulator in the biosynthesis of TA. Thus, the tempo-spatial transcription map we construct can help uncover the regulatory network during the root development of *S. miltiorrhiza* and verify novel regulators of major metabolic pathways and other major biological processes.

4. Discussion

As diterpenoid components in the *S. miltiorrhiza* root, tanshinones are specifically biosynthesized and accumulated in the periderm of the root. We found they were gradually synthesized in the seedling stage with the root changes from white to red, and characterized the spatiotemporal accumulation pattern in *S. miltiorrhiza* by transcript profiles, metabolite features, and chromatin accessibility. When the plant reaches a certain stage of development, the switch is turned on, and the biosynthesis of secondary metabolites is produced step by step. The specificity of development and spatial distribution suggests sophisticated and exquisite regulatory mechanisms in *S. miltiorrhiza*. 211 candidates were chosen with potential involvement in the exquisite regulatory process. Among them, SmERF105 was revealed to co-regulate the biosynthesis and transport of tanshinones.

The function of ERF105 has been reported to be predominantly associated with stress resistance and the regulation of small-molecule biosynthesis and transport. ERF105 makes a significant contribution to freezing tolerance and cold acclimation in *Arabidopsis thaliana* and *Cassava*[36,37]. It may act in conjunction with the well-known CBF regulon. VviERF105 is involved in response to abiotic stresses (freezing, drought, and salt) in *Vitis vinifera* L[38]. ERF105 is predicted to be associated with anthocyanin biosynthesis in *Crataegus maximowiczii*[39]. The phytopathogen *Pseudomonas syringae* delivers into host cells type III secreted effectors that promote virulence. ERF105 displayed a role in defense against *P. syringae*[40]. Besides, VvERF105 regulates the expression of the sugar transporter gene *VvSWEET15* in grapevine[41]. We have discovered that ERF105 functions in the coordinated regulation of tanshinone biosynthesis and transport in *S. miltiorrhiza*, expanding the known functions of ERF transcription factors. In this study, *S. miltiorrhiza* seedlings with knocked-out ERF105 were transplanted and grown for two months. No significant differences in growth and development were observed compared to wild-type plants (Supporting Information Fig. S10); therefore, we focused solely on quantifying the tanshinone content in the roots and did not systematically investigate the impact of ERF105 on plant growth and development. Although the role of ERF105 in plant growth and development was not examined, we cannot exclude its potential regulatory functions in the growth, development, and environmental adaptation of *S. miltiorrhiza.* This aspect warrants further investigation.

To date, several families of transcriptional regulators have been identified that regulate the transcriptional levels of tanshinone pathway genes and thereby affect biosynthesis[8,21,35,42-44]. Some of them function in specific biological contexts, for example, in response to the induction of signaling molecules such as jasmonic acids[45]. Several transcription factors may act at different hierarchical levels, sensing the external ecological environment and their developmental processes to carry out precise regulation. Regulatory architecture operates as a non-linear, interconnected network rather than a linear hierarchy of control nodes. Critical knowledge gaps persist regarding the topological relationships among these regulators, particularly in distinguishing direct protein−protein interactions (*e.g.*, transcription factor complex formation) from indirect epistatic regulatory cascades mediated by intermediate signaling molecules. Furthermore, the potential pleiotropic effects of these factors—whether they coordinate tanshinone biogenesis with other physiological processes through *trans*-regulatory crosstalk (*e.g.*, jasmonate signaling or redox homeostasis)—represent an unexplored dimension of metabolic regulation. Decrypting this multilayered interactome will illuminate evolutionarily conserved metabolic strategies in plants and reveal how sessile organisms dynamically optimize secondary metabolite synthesis in response to ecological pressures, potentially informing the design of stress-resilient metabolic engineering platforms.

The genes encoding members of the biosynthetic pathways of over 30 plant secondary metabolites are known to be present in BGCs[46,47]. In addition to metabolic pathway genes, it has been

(C) Dual-luc assays showing the activation capacity of ERF105 on the promoters of the target gene. $*P < 0.05$. (D) Schematic diagram of constructing erf105 mutants using the CRISPR/Cas9 editing system. A 100 bp fragment was subjected to being knocked out. (E) The transcription levels of *CYP76AH3*, *ABCG1*, and *KSL1* in *erf105* mutant lines were significantly reduced. (F) The contents of the four tanshinones in the *erf105* mutant lines were significantly decreased. Values are means ± SD ($n = 3$). $*P < 0.05$, $**P < 0.01$, and $***P < 0.001$ (Student's *t*-test).

discovered that transporters for secondary metabolites are clustered with their biosynthetic genes, as exemplified by the cucurbitacin transporters in *Cucurbitaceae* and tanshinone transporters in *Salvia* species[16,48]. Two hypotheses have been proposed for how these gene clusters formed. One hypothesis suggests that co-inheritance of these genes *via* colocalization prevents the loss of key genes in these pathways. The other hypothesis proposes that genes within the same BGC share the same promoters or cis-regulatory elements, thereby ensuring the coordinated production of biosynthetic enzymes and optimizing the yield of the final product[49-51]. Here, we discovered that SmERF105 can co-regulate pathway genes *KSL1* and *CYP76AH3*, and the transporter coding gene *ABCG1*. It represents an efficient strategy to manage specialized metabolites in plants. Plants produce a vast array of specialized metabolites that help them solve ecological challenges[52]. How plants balance stress resistance and autotoxicity has long been a fundamental question in plant science. On one hand, plants mitigate autotoxicity through structural modifications of secondary metabolites. For instance, certain diterpenes in tobacco exhibit cytotoxicity but are detoxified *via* hydroxylation, thereby reducing their toxicity to the plant itself while enhancing their insecticidal effect against herbivores[52]. On the other hand, plants compartmentalize secondary metabolites into specific subcellular locations to alleviate cytotoxicity, as observed in the vacuolar sequestration of alkaloids[53]. Here, we identify a dual-function transcription factor that coordinately regulates both the biosynthesis and transport of tanshinones, suggesting a potential efficient mechanism for mitigating autotoxicity in *S. miltiorrhiza*.

The functional enrichment of genes expressed at different growth stages suggests that plants initiate the process of secondary metabolite biosynthesis around 25 days after germination. This timing appears to be a critical juncture for metabolic diversification. Differential gene annotation of chromatin accessibility further revealed that the biosynthesis process of secondary metabolites in plants remains highly active in the later stages of development, particularly around 25 days. Notably, this stage coincides with the formation of secondary structures in plant roots, such as the development of vascular tissues and lignification processes. We speculate that there is a close relationship between plant secondary metabolites and the development of secondary structures. Secondary metabolites, such as flavonoids and lignins, may play essential roles in the structural integrity and defense mechanisms of these tissues[54-56]. Understanding how plants coordinate the construction of plant tissues with the biosynthesis of metabolic products is an intriguing question worth exploring. This coordination likely involves complex regulatory networks that integrate hormonal signaling, transcriptional regulation, and epigenetic modifications to ensure optimal resource allocation and developmental outcomes. Future research should focus on elucidating these regulatory mechanisms to gain deeper insights into plant development and metabolism.

In addition to chromatin accessibility, there are other multifaceted regulatory mechanisms, such as three-dimensional genome information and a series of modifications like histone modifications[51,57]. Literature reports that DNA methylation modifications can affect the biosynthesis of active secondary metabolites in *S. miltiorrhiza*[58]. Different dimensional regulatory mechanisms work together to precisely regulate the biosynthesis and transport of plant secondary metabolites, and more abundant multi-dimensional regulatory mechanisms still need further research.

5. Conclusions

In this study, we revealed the spatiotemporal metabolism of tanshinones in *S. miltiorrhiza* roots. Both transcriptome and ATAC profiles indicated the transition from primary metabolite to secondary metabolite in the seedling roots, with red tanshinones emerging across this process. Integrating information in the temporal and spatial dimensions, 211 TF candidates were predicted to mediate the "swatch" that regulates the accumulation of tanshinones in the periderm of roots. A novel TF was shown to co-regulate biosynthesis and transport of tanshinones in *S. miltiorrhiza*. Collectively, this study highlighted spatiotemporal metabolism and the potential regulatory mechanisms of diterpenes in plants.

Acknowledgments

This work was financially supported by the National Natural Science Foundation of China (82304662), National Key Research and Development Program of China (2022YFC3501700), "Chen Guang" project supported by Shanghai Municipal Education Commission and Shanghai Education Development Foundation (23CGA52, China), National Natural Science Foundation of China (82374159), National Key Research and Development Program of China (2023YFC3504800), Science and Technology Development Program of Shanghai University of Traditional Chinese Medicine (23KFL051, China), and Shanghai Municipal Science and Technology Commission (23XD1423500, China). We also thank Pro. Jun Xiao from the Chinese Academy of Sciences for the advice on pseudotime analyses.

Author contributions

Junfeng Chen, Wansheng Chen, Ying Xiao, and Lei Zhang conceived and designed the entire research plan. Yajing Li performed the experiments and wrote the manuscript. Peng Di, Yinan Zou, Xiao Li, Ke Zhang, and Jing Wang performed bioinformatic analyses. Shi Qiu and Yun Wang performed metabolic analysis. Weixu Chen, Jingfu Tan, Bo Li, and Tingzhao Li assisted in the experiments.

Conflicts of interest

The authors declare no conflicts of interest.

Data and availability

The data supporting this work is available. All raw sequencing data are stored in the biological project library (https://ngdc.cncb.ac.cn/bioproject/). RNA-seq: PRJCA038604 and PRJCA038480. ATAC-seq: PRJCA012883.

Appendix A. Supporting information

Supporting information to this article can be found online at https://doi.org/10.1016/j.apsb.2025.12.018.

References

1. Sargazifar Z, Ghorbanian Charami D, Esmaeilzadeh Kashi M, Asili J, Shakeri A. Abietane-type diterpenoids: insights into structural

diversity and therapeutic potential. *Chem Biodivers* 2024;**21**: e202400808.
2. Chen J, Wei X, Zhang Q, Wu Y, Xia G, Xia H, et al. The traditional Chinese medicines treat chronic heart failure and their main bioactive constituents and mechanisms. *Acta Pharm Sin B* 2023;**13**:1919−55.
3. Ma Y, Cui G, Chen T, Ma X, Wang R, Jin B, et al. Expansion within the CYP71D subfamily drives the heterocyclization of tanshinones synthesis in *Salvia miltiorrhiza. Nat Commun* 2021;**12**:685.
4. Song JJ, Fang X, Li CY, Jiang Y, Li JX, Wu S, et al. A 2-oxoglutarate-dependent dioxygenase converts dihydrofuran to furan in Salvia diterpenoids. *Plant Physiol* 2022;**188**:1496−506.
5. Xian Y, Zhang J, Bian Z, Zhou H, Zhang Z, Lin Z, et al. Bioactive natural compounds against human coronaviruses: a review and perspective. *Acta Pharm Sin B* 2020;**10**:1163−74.
6. Zhu Y, Ouyang Z, Du H, Wang M, Wang J, Sun H, et al. New opportunities and challenges of natural products research: when target identification meets single-cell multiomics. *Acta Pharm Sin B* 2022; **12**:4011−39.
7. Wu X, Liu L, Zheng Q, Ye H, Yang H, Hao H, et al. Dihydrotanshinone I preconditions myocardium against ischemic injury *via* PKM2 glutathionylation sensitive to ROS. *Acta Pharm Sin B* 2023;**13**: 113−27.
8. Wang Z, Peters RJ. Tanshinones: leading the way into Lamiaceae labdane-related diterpenoid biosynthesis. *Curr Opin Plant Biol* 2022; **66**:102189.
9. Li CY, Yang L, Liu Y, Xu ZG, Gao J, Huang YB, et al. The sage genome provides insight into the evolutionary dynamics of diterpene biosynthesis gene cluster in plants. *Cell Rep* 2022;**40**:111236.
10. Cheng Y, Luo L, Tang H, Wang J, Ren L, Cui G, et al. Engineering the microenvironment of P450s to enhance the production of diterpenoids in Saccharomyces cerevisiae. *Acta Pharm Sin B* 2024;**14**: 4608−18.
11. Mao L, Jin B, Chen L, Tian M, Ma R, Yin B, et al. Functional identification of the terpene synthase family involved in diterpenoid alkaloids biosynthesis in Aconitum carmichaelii. *Acta Pharm Sin B* 2021;**11**:3310−21.
12. Cheng Q, Su P, Hu Y, He Y, Gao W, Huang L. RNA interference-mediated repression of SmCPS (copalyldiphosphate synthase) expression in hairy roots of *Salvia miltiorrhiza* causes a decrease of tanshinones and sheds light on the functional role of SmCPS. *Biotechnol Lett* 2014;**36**:363−9.
13. Cui G, Duan L, Jin B, Qian J, Xue Z, Shen G, et al. Functionaldivergence of diterpene syntheses in the medicinal plant *Salvia miltiorrhiza. Plant Physiol* 2015;**169**:1607−18.
14. Guo J, Ma X, Cai Y, Ma Y, Zhan Z, Zhou YJ, et al. Cytochrome P450 promiscuity leads to a bifurcating biosynthetic pathway for tanshinones. *New Phytol* 2016;**210**:525−34.
15. Guo J, Zhou YJ, Hillwig ML, Shen Y, Yang L, Wang Y, et al. CYP76AH1 catalyzes turnover of miltiradiene in tanshinones biosynthesis and enables heterologous production of ferruginol in yeasts. *Proc Natl Acad Sci U S A* 2013;**110**:12108−13.
16. Li Y, Chen J, Zhi J, Huang D, Zhang Y, Zhang L, et al. The ABC transporter SmABCG1 mediates tanshinones export from the peridermic cells of *Salvia miltiorrhiza* root. *J Integr Plant Biol* 2025;**67**: 135−49.
17. Kazachkova Y, Zemach I, Panda S, Bocobza S, Vainer A, Rogachev I, et al. The GORKY glycoalkaloid transporter is indispensable for preventing tomato bitterness. *Nat Plants* 2021;**7**:468−80.
18. Li Y, Chen Y, Zhou L, You S, Deng H, Chen Y, et al. MicroTom metabolic network: rewiring tomato metabolic regulatory network throughout the growth cycle. *Mol Plant* 2020;**13**:1203−18.
19. Fu BL, Wang WQ, Li X, Qi TH, Shen QF, Li KF, et al. A dramatic decline in fruit citrate induced by mutagenesis of a NAC transcription factor, AcNAC1. *Plant Biotechnol J* 2023;**21**:1695−706.
20. Shi M, Liao P, Nile SH, Georgiev MI, Kai G. Biotechnological exploration of transformed root culture for value-added products. *Trends Biotechnol* 2021;**39**:137−49.
21. Zheng H, Fu X, Shao J, Tang Y, Yu M, Li L, et al. Transcriptional regulatory network of high-value active ingredients in medicinal plants. *Trends Plant Sci* 2023;**28**:429−46.
22. Qiu S, Tu Y, Huang D, Dong Z, Huang M, Cheng J, et al. Selection of appropriate post-harvest processing methods based on the metabolomics analysis of *Salvia miltiorrhiza* Bunge. *Food Res Int* 2021;**144**: 110366.
23. Liu X, Bie XM, Lin X, Li M, Wang H, Zhang X, et al. Uncovering the transcriptional regulatory network involved in boosting wheat regeneration and transformation. *Nat Plants* 2023;**9**:908−25.
24. Killcoyne S, Carter GW, Smith J, Boyle J. Cytoscape: a community-based framework for network modeling. *Methods Mol Biol* 2009; **563**:219−39.
25. Langmead B, Salzberg SL. Fast gapped-read alignment with Bowtie 2. *Nat Methods* 2012;**9**:357−9.
26. Zhang Y, Liu T, Meyer CA, Eeckhoute J, Johnson DS, Bernstein BE, et al. Model-based analysis of ChIP-Seq (MACS). *Genome Biol* 2008; **9**:R137.
27. Robinson JT, Thorvaldsdottir H, Turner D, Mesirov JP. igv.js: an embeddable JavaScript implementation of the Integrative Genomics Viewer (IGV). *Bioinformatics* 2023;**39**:btac830.
28. Xie K, Minkenberg B, Yang Y. Boosting CRISPR/Cas9 multiplex editing capability with the endogenous tRNA-processing system. *Proc Natl Acad Sci U S A* 2015;**112**:3570−5.
29. Niu Q, Wu S, Xie H, Wu Q, Liu P, Xu Y, et al. Efficient A·T to G·C base conversions in dicots using adenine base editors expressed under the tomato EF1α promoter. *Plant Biotechnol J* 2023;**21**:5−7.
30. Yao Y, Zhou J, Wang J, Lei X, Jiang A, Sun Q. H3K36 methylation stamps transcription resistive to preserve development in plants. *Nat Plants* 2025;**11**:808−20.
31. Lin X, Xu Y, Wang D, Yang Y, Zhang X, Bie X, et al. Systematic identification of wheat spike developmental regulators by integrated multi-omics, transcriptional network, GWAS, and genetic analyses. *Mol Plant* 2024;**17**:438−59.
32. Jin J, Tian F, Yang DC, Meng YQ, Kong L, Luo J, et al. PlantTFDB 4.0: toward a central hub for transcription factors and regulatory interactions in plants. *Nucleic Acids Res* 2017;**45**:D1040−5.
33. Bai Z, Wu J, Huang W, Jiao J, Zhang C, Hou Z, et al. The ethylene response factor SmERF8 regulates the expression of SmKSL1 and is involved in tanshinone biosynthesis in *Saliva miltiorrhiza* hairy roots. *J Plant Physiol* 2020;**244**:153006.
34. Bai Z, Li W, Jia Y, Yue Z, Jiao J, Huang W, et al. The ethylene response factor SmERF6 co-regulates the transcription of SmCPS1 and SmKSL1 and is involved in tanshinone biosynthesis in *Salvia miltiorrhiza* hairy roots. *Planta* 2018;**248**:243−55.
35. Li Y, Cao J, Zhang Y, Liu Y, Gao S, Zhang P, et al. The methyl jasmonate-responsive transcription factor SmERF106 promotes tanshinone accumulation in *Salvia miltiorrhiza. Plant Physiol Biochem* 2024;**214**:108932.
36. Yu G, Zhang B, Chen Q, Huang Z, Zhang B, Wang K, et al. Dynamic DNA methylation modifications in the cold stress response of cassava. *Genomics* 2024;**116**:110871.
37. Bolt S, Zuther E, Zintl S, Hincha DK, Schmülling T. ERF105 is a transcription factor gene of *Arabidopsis thaliana* required for freezing tolerance and cold acclimation. *Plant Cell Environ* 2017;**40**:108−20.
38. Wang L, Zhang X, Qu Z, Guo W, Van NS, Zhang C. Grapevine VviERF105 promotes tolerance to abiotic stress and is degraded by the E3 ubiquitin ligase VviPUB19. *Environ Exp Bot* 2022;**201**:105001.
39. Zhang X, Wang J, Li P, Sun C, Dong W. Integrative metabolome and transcriptome analyses reveals the black fruit coloring mechanism of *Crataegus maximowiczii* C. K. Schneid. *Plant Physiol Biochem* 2023; **194**:111−21.
40. Cao FY, Khan M, Taniguchi M, Mirmiran A, Desveaux D. A host−pathogen interactome uncovers phytopathogenic strategies to manipulate plant ABA responses. *Plant J* 2019;**100**:187−98.
41. Lu L, Delrot S, Fan P, Zhang Z, Wu D, Dong F, et al. The transcription factors ERF105 and NAC72 regulate expression of a sugar

transporter gene and hexose accumulation in grape. *Plant Cell* 2024; **37**:koae326.
42. Cao R, Lv B, Shao S, Zhao Y, Yang M, Zuo A, et al. The SmMYC2−SmMYB36 complex is involved in methyl jasmonate-mediated tanshinones biosynthesis in *Salvia miltiorrhiza. Plant J* 2024;**119**:746−61.
43. Zheng H, Fu X, Yu M, Liu Q, Li C, Li L, et al. Transcriptome and yeast two-hybrid sequencing shed light on the crosstalk between light and jasmonate signaling in regulating tanshinone biosynthesis. *Med Plant Biol* 2024;**3**:e006. 0-13.
44. Wang X, Shi Y, Wang Q, Xie X, Gui S, Wu J, et al. Molecular mechanism of SmMYB53 activates the expression of SmCYP71D375, thereby modulating tanshinone accumulation in *Salvia miltiorrhiza. Hortic Res* 2025;**12**:uhaf058.
45. Li W, Lin S, Wang R, Chen C, Ni L, Wang W, et al. Regulation of plant hormones on the secondary metabolism of medicinal plants. *Med Plant Biol* 2025;**4**:e020. 0-10.
46. Sasse J, Simon S, Gübeli C, Liu GW, Cheng X, Friml J, et al. Asymmetric localizations of the ABC transporter PaPDR1 trace paths of directional strigolactone transport. *Curr Biol* 2015;**25**: 647−55.
47. Zhao D, Zhang Y, Ren H, Shi Y, Dong D, Li Z, et al. Multi-omics analysis reveals the evolutionary origin of diterpenoid alkaloid biosynthesis pathways in Aconitum. *J Integr Plant Biol* 2023;**65**: 2320−35.
48. Zhong Y, Xun W, Wang X, Tian S, Zhang Y, Li D, et al. Root-secreted bitter triterpene modulates the rhizosphere microbiota to improve plant fitness. *Nat Plants* 2022;**8**:887−96.
49. Bryson AE, Lanier ER, Lau KH, Hamilton JP, Vaillancourt B, Mathieu D, et al. Uncovering a miltiradiene biosynthetic gene cluster in the Lamiaceae reveals a dynamic evolutionary trajectory. *Nat Commun* 2023;**14**:343.
50. Takos AM, Rook F. Why biosynthetic genes for chemical defense compounds cluster. *Trends Plant Sci* 2012;**17**:383−8.
51. Yang X, Gao S, Guo L, Wang B, Jia Y, Zhou J, et al. Three chromosome-scale Papaver genomes reveal punctuated patchwork evolution of the morphinan and noscapine biosynthesis pathway. *Nat Commun* 2021;**12**:6030.
52. Li J, Halitschke R, Li D, Paetz C, Su H, Heiling S, et al. Controlled hydroxylations of diterpenoids allow for plant chemical defense without autotoxicity. *Science* 2021;**371**:255−60.
53. Morita M, Shitan N, Sawada K, Van Montagu MC, Inzé D, Rischer H, et al. Vacuolar transport of nicotine is mediated by a multidrug and toxic compound extrusion (MATE) transporter in Nicotiana tabacum. *Proc Natl Acad Sci U S A* 2009;**106**:2447−52.
54. Jahan T, Huda MN, Zhang K, He Y, Lai D, Dhami N, et al. Plant secondary metabolites against biotic stresses for sustainable crop protection. *Biotechnol Adv* 2025;**79**:108520.
55. Zhou S, Ma Y, Shang Y, Qi X, Huang S, Li J. Functional diversity and metabolic engineering of plant-specialized metabolites. *Life Metab* 2022;**1**:109−21.
56. Huang AC, Jiang T, Liu YX, Bai YC, Reed J, Qu B, et al. A specialized metabolic network selectively modulates *Arabidopsis* root microbiota. *Science* 2019;**364**:eaau6389.
57. Liu M, Yue Y, Chen X, Xian K, Dong C, Shi M, et al. Genome-coverage single-cell histone modifications for embryo lineage tracing. *Nature* 2025;**640**:828−39.
58. Li J, Li C, Deng Y, Wei H, Lu S. Characteristics of *Salvia miltiorrhiza* methylome and the regulatory mechanism of DNA methylation in tanshinone biosynthesis. *Hortic Res* 2023;**10**:uhad114.